Wavenumber-4 patterns of the total electron content over the low latitude ionosphere

W. Wan,[1] L. Liu,[1] X. Pi,[2] M.-L. Zhang,[1] B. Ning,[1] J. Xiong,[1] and F. Ding[1]

[1] The global ionospheric maps (GIMs) produced by JPL are used to investigate the longitudinal structure of the low latitude ionosphere. As a proxy of the ionization parameter at low latitudes, the latitudinally integrated total electron content (ITEC) is first extracted from low latitude GIMs and then Fourier filtered to obtain the wavenumber-4 components. We then study in detail the diurnal, seasonal and solar cycle variations of the wave patterns. It is found that the wavenumber-4 patterns are intense and well developed in boreal summer and early boreal autumn, but quite weak in boreal winter. This seasonal variation is consistent with that of the zonal wind of the non-migrating tide mode DE3. We also found that the wavenumber-4 patterns shift eastward with a shifting speed that is smaller in daytime than at night. This is attributed to the contribution of both the eastward propagation of DE3 in E-region and the zonal $\mathbf{E} \times \mathbf{B}$ ion drifts in F-region. Our results support the suggestion that the longitudinal wavenumber-4 structure of the low latitude ionosphere should be originated from the non-migrating tide mode DE3. **Citation:** Wan, W., L. Liu, X. Pi, M.-L. Zhang, B. Ning, J. Xiong, and F. Ding (2008), Wavenumber-4 patterns of the total electron content over the low latitude ionosphere, *Geophys. Res. Lett.*, *35*, L12104, doi:10.1029/2008GL033755.

1. Introduction

[2] It was recently noticed that the low-latitude ionosphere shows a remarkable longitudinal wavenumber-4 patterns, i.e., the equatorial ionospheric anomaly (EIA) crests are enhanced over West Africa, Southeast Asia, Central Pacific Ocean and South America. Analyzing IMAGE-FUV observations, *Sagawa et al.* [2005] first reported that the intensity of the nightglow emission at 135.6 nm, proportional to square of the F-region electron density, is enhanced at four longitudes separated about 90° from each other. Similar results appear also in the TIMED-GUVI observations at the same emission [*Henderson et al.*, 2005]. *England et al.* [2006a] compared both the FUV and the GUVI observations and demonstrated that the wavenumber-4 structure persists in the post sunset ionosphere and lasts at least until midnight over months. *Lin et al.* [2007a] analyzed the electron density profiles observed by radio occultation from FORMOSAT-3/COSMIC satellites and found that the wavenumber-4 patterns occurs usually at altitudes above 250 km. *Lin et al.* [2007b] also studied the diurnal variation of the wavenumber-4 patterns and pointed out that they may also appear in daytime. Using the long duration TEC data measured by the TOPEX/Poseidon altimeter, *Scherliess et al.* [2008] found that the wavenumber-4 patterns created during the daytime hours undergo a remarkable seasonal variation, but are largely independent of the solar cycle conditions. Besides the ionospheric ionization, the longitudinal wavenumber-4 structure also occurred in other parameters such as the vertical ion drift velocity, the electron temperature, and even in the zonal neutral wind in the F region [*Hartman and Heelis*, 2007; *Ren et al.*, 2008; *Kil et al.*, 2007; *Häusler et al.*, 2007; *Lühr et al.*, 2007].

[3] The effect of the coupling process between the ionosphere and the atmosphere below has been considered as the physical mechanism responsible for the observed longitudinal wavenumber-4 structure. *Sagawa et al.* [2005] postulated that the E-region non-migrating semidiurnal tide [*Hagan and Forbes*, 2003] should be the origin of the wavenumber-4 structure in F-region. *England et al.* [2006b] further demonstrated a clear correspondence between the non-migrating diurnal tides [*Hagan and Forbes*, 2002] and the morphology of the post sunset EIA. *Immel et al.* [2006] discussed in detail the production of the wavenumber-4 patterns by the longitudinal modulation of the F-region fountain effects which is created in turn by the longitudinal modulation of the non-migrating diurnal tide on the E-region dynamo. Using the NCAR TIME-GCM model, *Hagan et al.* [2007] reproduced the wavenumber-4 patterns as a result of the effects of an eastward propagating zonal wavenumber-3 diurnal tide (DE3).

[4] The present work uses the global observations of ionospheric total electron content (TEC) to study the longitudinal wavenumber-4 structure over the low latitude ionosphere. Long period TEC data from the global ionospheric maps (GIMs) produced by JPL are used to extract the latitudinally integrated TEC (ITEC) which is considered as a proxy of the ionization parameter at low latitudes, mostly in the EIA region. The wavenumber-4 component filtered from the extracted ITEC data is further used to investigate its diurnal, seasonal and solar cycle variations. Our results support the suggestion that the longitudinal wavenumber-4 structure should be originated from the non-migrating tide DE3.

2. Data and Analysis

[5] Global ionospheric maps (GIMs) for ionospheric TEC have been routinely produced by JPL since 1998 [e.g., *Mannucci et al.*, 1998; *Iijima et al.*, 1999]. A GIM provides a snapshot of TEC by interpolating TEC measure-

---

[1]Institute of Geology and Geophysics, Chinese Academy of Sciences, Beijing, China.
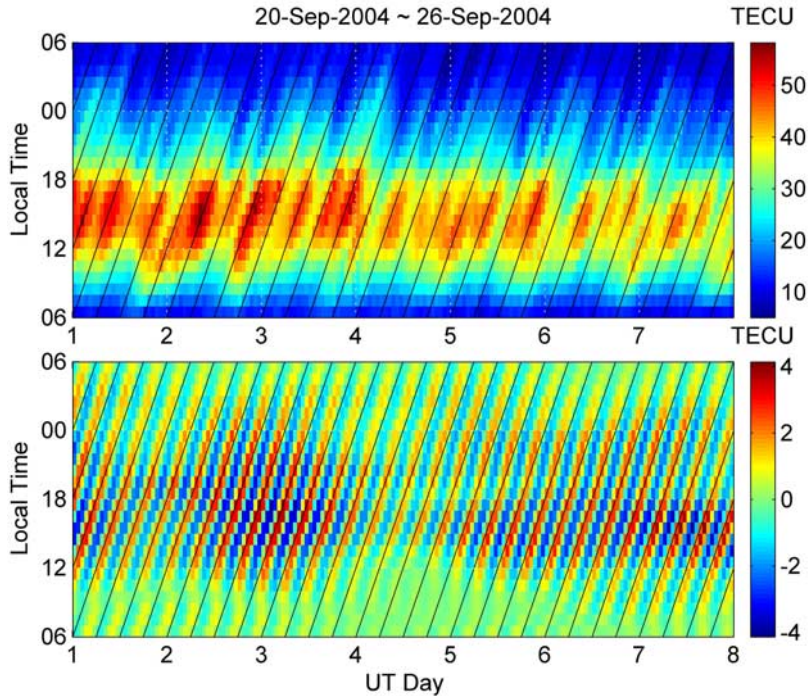[2]Jet Propulsion Laboratory, California Institute of Technology, Pasadena, California, USA.

Figure 1. A segment of latitudinally integrated TEC (ITEC) as a function of local time (in hour) and UT day. The top plot shows the original data sorted from the JPL GIMs during a 7-day interval at and near the September equinox in 2004 (20–26, September, 2004). The bottom plot shows the Fourier filtered wavenumber-4 component. The straight slanted lines in both plots indicate the constant longitude with a 90° step.

ments from about 100 GPS receivers (the number was doubled since April 5, 2004). Each of the receivers may provide 6–8 simultaneous TEC measurements in locations over the station within about 1000 km horizontal range, and the total number of the simultaneous observations may reach to about 700 (or 1400) points. Thus a GIM is reconstructed with very large amount of data points which ensure a very high average spatial resolution. Furthermore, most of the GPS receivers are located in the continents and some on islands, the station locations were selected on purpose to cover the world, including both lands and oceans, as evenly as possible. Thus for most regions the resolution of the observation point may satisfy the requirement for describing the wavenumber-4 structure, although there exist considerable gaps in some ocean regions (especially in Central Pacific region). The present work uses the version of GIM with spatial resolution of 5° × 2.5° (longitude × latitude) and temporal resolution of 2 hours (UT), which is archived at the website ftp://cddisa.gsfc.nasa.gov/gps/products/ionex/.

[6] To analyze these data, we consider the snapshot TEC as a function of longitude (*Lon*, in degrees), latitude (*Lat*, in degrees), universal time (*UT*, in hours), and day, and perform the latitudinal integration of TEC from low latitude GIMs,

$$ITEC(Lon, UT, day) = \frac{1}{Lat_N - Lat_S} \int_{Lat_S}^{Lat_N} \cdot TEC(Lon, Lat, UT, day) dLat$$

where the integration is carried within ±30° magnetic latitudes, and for convenience we normalize the integration (divided by $Lat_N - Lat_S$) hence ITEC is actually the average of TEC in EIA region. We further sort ITEC according to local time ($LT = Lon/15 + UT$, in hours) and UT days ($UTday = UT/24 + day$, in days). Thus in the LT-frame, the resulted *ITEC(LT, UTday)* is considered as a set of time series (here the time refers UT days) measured by sun-synchronous observers in different local time.

[7] An example of ITEC is shown in the top plot of Figure 1, which presents a LT-dependent time series of ITEC during a 7-day interval at and near the September Equinox in 2004. It is clear that ITEC not only undergoes the LT variation but also changes with UT day. For a given LT the ITEC variation with UT days also reflects longitudinal structures since $Lon = LT/24 - UTday$ (in cycles). To obtain the longitudinal wavenumber spectra, we perform a spectral analysis on the time series *ITEC(LT, UTday)*. As an example, Figure 2 shows the LT-dependent spectral amplitude calculated from the Fourier transform on the ITEC data shown in the top plot of Figure 1. The estimated spectra illustrate a pronounced 'tidal' structure for the ITEC variations with UT day (or longitude), and the wavenumber-4 is quite remarkable among the different 'tidal' components.

[8] Our primary interest is in the wavenumber-4 structure. This component is picked out by the inverse Fourier transformation on the obtained spectra in a wavenumber band from 3.5 to 4.5, as indicated by the broken rectangle in Figure 2. The bottom plot of Figure 1 depicts the Fourier filtered wavenumber-4 patterns of ITEC corresponding to the original data shown in the top plot. The filtered patterns
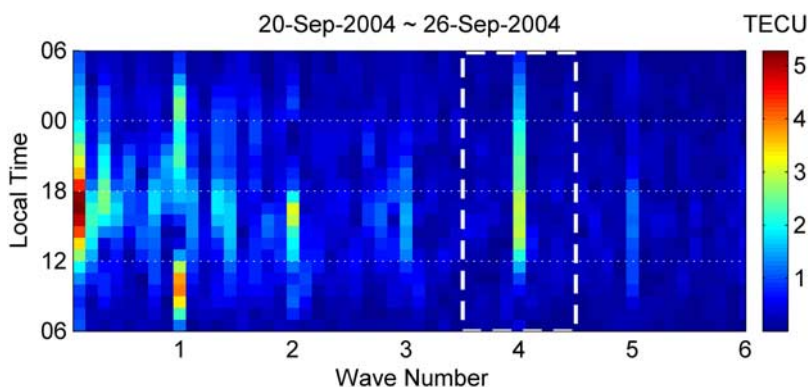
Figure 2. The amplitude of the LT-dependent wavenumber spectra calculated from the data in the top plot of Figure 1. The white broken rectangle denotes the boundary of a band pass filter used in calculating the wavenumber-4 patterns illustrated in the bottom plot of Figure 1.

persist in the whole selected segment although there is a day to day variability.

3. Results and Discussion

[9] With the procedure introduced above, we processed the TEC data from JPL GIMs observed during the period from August 1998 to the end of 2007, which covers the solar activities from high to low level. The Fourier filtered wavenumber-4 component of the ITEC data is averaged according to different levels of solar flux (presented by F107) and different months, and the results of ITEC maps vs. longitude and local time are displayed in Figure 3. Because of the recurrence of the wave patterns in the longitude domain, Figure 3 gives only the one-pattern ITEC maps (i.e., the maps in a longitude range from $-45°$ to $45°$ hence containing only one wave pattern in each map). The three rows from top to bottom show the results for the low (F107 < 120), medium (120 < F107 < 160) and high (F107 > 160) solar flux levels, respectively. The columns from left to right are respectively for the twelve months from January through December. The contours in the maps illustrate the absolute values of ITEC equal to the standard deviation of the wave field; hence their corresponding locations indicate where the wave patterns are remarkable.

[10] From Figure 3 it is seen that the intensity of the wavenumber-4 patterns depends very much on season and also slightly on solar activity. For the low solar flux conditions (the top plots in Figure 3), the patterns are very weak and not well developed in boreal winter (December to February). The patterns begin to appear in March and then become well developed in April and May. They start either at the noontime (in March and April) or in the forenoon (in May), and become intense in the afternoon and last to post sunset (in March) or even to the midnight (in April and May). During boreal summer (June through August), the wave patterns are very intense and well developed. They appear in the later morning (0900 LT), become very strong in the afternoon and post sunset, and last to pre-midnight. In boreal autumn (September through November) the wave intensity is still very strong. In fact, it is even more enhanced in September, and then decreased rapidly in October and November. In summary, the wave intensity is weak in boreal winter and strong in boreal summer and

early autumn; it is increased in boreal spring and decreased rapidly in later boreal autumn.

[11] It can be seen in Figure 3 that the increase of the solar flux modifies slightly the seasonal variations of the intensity of the wavenumber-4 patterns. For medium and high solar flux (middle and bottom plots in Figure 3), the wave intensity is still very weak and the wave patterns are also undeveloped in boreal winter. In fact, the wave patterns are not yet well developed even in early boreal spring (March and April) and later boreal autumn (November) for medium solar activity. In contrast, the wave patterns are very much enhanced and well developed during boreal summer and early autumn; both the intensity and the lasting duration of the wavenumber-4 patterns are increased with solar flux.

[12] As suggested by previous works [*Sagawa et al.*, 2005; *England et al.*, 2006a; *Immel et al.*, 2006; *Hagan et al.*, 2007], the longitudinal wavenumber-4 structure in the EIA region may be caused by the longitudinal modulation of the F-region ion drifts which is created in turn by the longitudinal modulation of the non-migrating tides on the E-region dynamo. It is largely believed that the main contributing tide is the DE3 mode (the eastward propagating zonal wavenumber-3 diurnal tide). Thus, the observed seasonal variation of the wavenumber-4 intensity should be corresponding to that of DE3 tide. Recently, the satellite observations reveal the seasonal climatology of non-migrating tides including DE3. With the HRDI and WINDII instruments on UARS, *Forbes et al.* [2003a, 2003b] found that the zonal wind of DE3 is stronger and occurs primarily during boreal summer and autumn, while the meridional component is relatively weaker and occurs during the boreal winter. Similar results are also obtained from the analysis of the TIDI data on board of the TIMED satellite [*Oberheide et al.*, 2006]. In addition, the observation from the TIMED-SEBER indicates that the seasonal change of the temperature fluctuation of DE3 is very similar to that of the zonal wind component [*Chen and Lu*, 2007; *Oberheide and Forbes*, 2008]. Therefore the seasonal variation of the ionospheric wavenumber-4 patterns is consistent completely with that of the zonal wind and temperature fluctuations of DE3, and has very little connection with that of the meridional wind component. As pointed out by *Oberheide and Forbes* [2008], the discrepancy in the seasonal variation
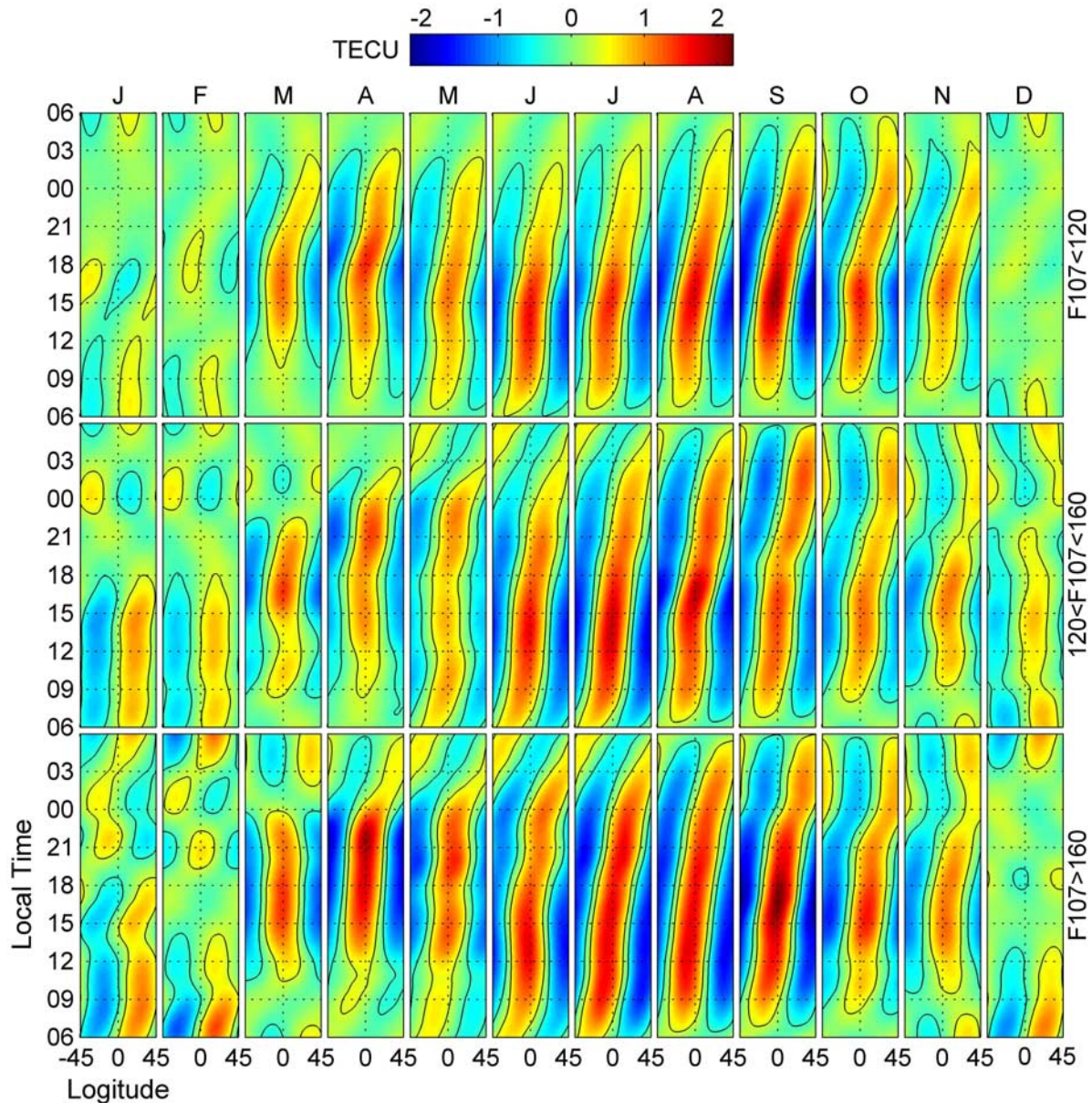
Figure 3. Mean patterns of the wavenumber-4 component filtered from the latitudinally integrated TEC (ITEC) of JPL GIMs. The three rows from top to bottom are respectively for low (F107 < 120), medium (120 < F107 < 160) and high (F107 > 160) levels of solar flux. The columns from left to right are respectively for months January through December. The contours depict the constant absolute value equal to the standard deviation of the wave field (about 0.68 TECU). Because of the recurrence of the wave patterns in the longitude domain, the figure shows only one-pattern ITEC maps in a longitude range from −45° to 45°.

between the DE3 components should be interpreted in terms of latitudinally symmetric versus antisymmetric modes (Hough modes). That is, the first symmetric mode, which occurs mainly in boreal summer and autumn, dominate the zonal wind component and the temperature fluctuation, and the first antisymmetric mode, which occurs mainly in boreal winter, dominate the meridional wind component. Hence our result about the seasonal climatology of the wavenumber-4 patterns implies the possibility that, in the coupling between the F-region ionosphere and the E-region atmosphere, the relatively stronger and more latitudinally symmetric zonal component of DE3 winds is more efficient

than the relatively weaker and more antisymmetric meridional component.

[13] Another important feature in Figure 3 is that the patterns of wavenumber-4 shift eastward as LT increases. The shifting speed (determined by the slope of the wave crests or valleys) changes with local time: it is usually small or occasionally change direction (to westward) in daytime, while it becomes very large around sunset and during nighttime. The eastward shift of the wavenumber-4 patterns may be at least of two origins. The first one is related to the eastward propagation of the causative non-migrating tides in the E-region. If we consider DE3 as the primary source of

our wavenumber-4 structure, the related shifting speed should be 120°/day in UT-frame, or 90°/day in LT-frame. By inspecting the slope of the wave patterns in Figure 3, we may find that the phase speed of DE3 (90°/day) is approximately the average shifting speed of our wavenumber-4 patterns. The deviation of the shifting speed from the phase speed of DE3 may be caused by the second origin, the zonal $\mathbf{E} \times \mathbf{B}$ drifts of the ions in the F-region. According to the observation of incoherent scatter radar, the zonal drifts are westward in daytime and eastward during night [*Fejer*, 1981; *Fejer et al.*, 2005], hence they reduce (or reverse) the eastward shifting of the wavenumber-4 patterns in daytime, and prick up the eastward shifting at night. Thus in Figure 3 the slop of the wave patterns is likely to be less (larger) than the DE3 phase velocity in daytime (at night).

4. Summary and Conclusion

[14] In the present work the JPL GIMs are used to obtain the longitudinal wavenumber-4 components of TEC variation at EIA latitudes. It is found that the intensity of the wavenumber-4 patterns depends very much on season. The seasonal variation of this wave component is that it is weak in boreal winter and strong in boreal summer and early autumn. We pointed out that such a seasonal variation is consistent with that of the zonal wind of the non-migrating tide DE3.

[15] It is also found that the wavenumber-4 patterns shift eastward. We explained the eastward shifting by both the phase propagation of DE3 in the E-region and the zonal $\mathbf{E} \times \mathbf{B}$ ion drift in the F-region. The mean shifting speed corresponds to the DE3 phase speed, and the deviation may result from the zonal ion drift. The diurnal variation of the shifting speed is consistent with that of the zonal $\mathbf{E} \times \mathbf{B}$ ion drift.

[16] In conclusion, our results support the suggestion that the non-migrating tide DE3 should be the origin of the observed longitudinal wavenumber-4 structure in the ionospheric F-region at EIA latitudes.

References

Chen, Z. Y., and D. R. Lu (2007), Seasonal variation of the MLT tides in 120°E meridian (in Chinese), *Acta Geophys. Sin.*, *50*, 691–700, *Chin. J. Geophys.*, Engl. Transl., *50*, 606–616.
England, S. L., T. J. Immel, E. Sagawa, S. B. Henderson, M. E. Hagan, S. B. Mende, H. U. Frey, C. M. Swenson, and L. J. Paxton (2006a), Effect of atmospheric tides on the morphology of the quiet time, postsunset equatorial ionospheric anomaly, *J. Geophys. Res.*, *111*, A10S19, doi:10.1029/2006JA011795.
England, S. L., S. Maus, T. J. Immel, and S. B. Mende (2006b), Longitudinal variation of the E-region electric fields caused by atmospheric tides, *Geophys. Res. Lett.*, *33*, L21105, doi:10.1029/2006GL027465.
Fejer, B. G. (1981), The equatorial ionospheric electric field. A review, *J. Atmos. Terr. Phys.*, *43*, 377–386.
Fejer, B. G., J. de Souza, A. S. Santos, and A. E. Costa Pereira (2005), Climatology of F region zonal plasma drifts over Jicamarca, *J. Geophys. Res.*, *110*, A12310, doi:10.1029/2005JA011324.
Forbes, J. M., M. E. Hagan, S. Miyahara, Y. Miyoshi, and X. Zhang (2003a), Diurnal nonmigrating tides in the tropical lower thermosphere, *Earth Planets Space*, *55*, 419–426.

Forbes, J. M., X. Zhang, E. R. Talaat, and W. Ward (2003b), Nonmigrating diurnal tides in the thermosphere, *J. Geophys. Res.*, *108*(A1), 1033, doi:10.1029/2002JA009262.
Hagan, M. E., and J. M. Forbes (2002), Migrating and nonmigrating diurnal tides in the middle and upper atmosphere excited by tropospheric latent heat release, *J. Geophys. Res.*, *107*(D24), 4754, doi:10.1029/2001JD001236.
Hagan, M. E., and J. M. Forbes (2003), Migrating and nonmigrating semi-diurnal tides in the upper atmosphere excited by tropospheric latent heat release, *J. Geophys. Res.*, *108*(A2), 1062, doi:10.1029/2002JA009466.
Hagan, M. E., A. Maute, R. G. Roble, A. D. Richmond, T. J. Immel, and S. L. England (2007), Connections between deep tropical clouds and the Earth's ionosphere, *Geophys. Res. Lett.*, *34*, L20109, doi:10.1029/2007GL030142.
Hartman, W. A., and R. A. Heelis (2007), Longitudinal variations in the equatorial vertical drift in the topside ionosphere, *J. Geophys. Res.*, *112*, A03305, doi:10.1029/2006JA011773.
Häusler, K., H. Lühr, S. Rentz, and W. Köhler (2007), A statistical analysis of longitudinal dependences of upper thermospheric zonal winds at dip equator latitudes derived from CHAMP, *J. Atmos. Sol. Terr. Phys.*, *69*, 1419–1430, doi:10.1016/j.jastp.2007.04.004.
Henderson, S. B., C. M. Swenson, A. B. Christensen, and L. J. Paxton (2005), Morphology of the equatorial anomaly and equatorial plasma bubbles using image subspace analysis of Global Ultraviolet Imager data, *J. Geophys. Res.*, *110*, A11306, doi:10.1029/2005JA011080.
Iijima, B. A., I. L. Harris, C. M. Ho, U. J. Lindqwister, A. J. Mannucci, X. Pi, M. J. Reyes, L. C. Sparks, and B. D. Wilson (1999), Automated daily process for global ionospheric total electron content maps and satellite ocean altimeter ionospheric calibration based on Global Positioning System data, *J. Atmos. Sol. Terr. Phys.*, *61*, 1205–1218.
Immel, T. J., E. Sagawa, S. L. England, S. B. Henderson, M. E. Hagan, S. B. Mende, H. U. Frey, C. M. Swenson, and L. J. Paxton (2006), Control of equatorial ionospheric morphology by atmospheric tides, *Geophys. Res. Lett.*, *33*, L15108, doi:10.1029/2006GL026161.
Kil, H., S.-J. Oh, M. C. Kelley, L. J. Paxton, S. L. England, E. Talaat, K.-W. Min, and S.-Y. Su (2007), Longitudinal structure of the vertical $\mathbf{E} \times \mathbf{B}$ drift and ion density seen from ROCSAT-1, *Geophys. Res. Lett.*, *34*, L14110, doi:10.1029/2007GL030018.
Lin, C. H., W. Wang, M. E. Hagan, C. C. Hsiao, T. J. Immel, M. L. Hsu, J. Y. Liu, L. J. Paxton, T. W. Fang, and C. H. Liu (2007a), Plausible effect of atmospheric tides on the equatorial ionosphere observed by the FORMOSAT-3/COSMIC: Three-dimensional electron density structures, *Geophys. Res. Lett.*, *34*, L11112, doi:10.1029/2007GL029265.
Lin, C. H., C. C. Hsiao, J. Y. Liu, and C. H. Liu (2007b), Longitudinal structure of the equatorial ionosphere: Time evolution of the four-peaked EIA structure, *J. Geophys. Res.*, *112*, A12305, doi:10.1029/2007JA012455.
Lühr, H., K. Häusler, and C. Stolle (2007), Longitudinal variation of F region electron density and thermospheric zonal wind caused by atmospheric tides, *Geophys. Res. Lett.*, *34*, L16102, doi:10.1029/2007GL030639.
Mannucci, A. J., B. D. Wilson, D. N. Yuan, C. M. Ho, U. J. Lindqwister, and T. F. Runge (1998), A global mapping technique for GPS-derived ionospheric total electron content measurements, *Radio Sci.*, *33*, 565–582.
Oberheide, J., and J. M. Forbes (2008), Tidal propagation of deep tropical cloud signatures into the thermosphere, *Geophys. Res. Lett.*, *35*, L04816, doi:10.1029/2007GL032397.
Oberheide, J., Q. Wu, T. L. Killeen, M. E. Hagan, and R. G. Roble (2006), Diurnal nonmigrating tides from TIMED Doppler Interferometer wind data: Monthly climatologies and seasonal variations, *J. Geophys. Res.*, *111*, A10S03, doi:10.1029/2005JA011491.
Ren, Z., W. Wan, L. Liu, B. Zhao, Y. Wei, X. Yue, and R. A. Heelis (2008), Longitudinal variations of electron temperature and total ion density in the sunset equatorial topside ionosphere, *Geophys. Res. Lett.*, *35*, L05108, doi:10.1029/2007GL032998.
Sagawa, E., T. J. Immel, H. U. Frey, and S. B. Mende (2005), Longitudinal structure of the equatorial anomaly in the nighttime ionosphere observed by IMAGE/FUV, *J. Geophys. Res.*, *110*, A11302, doi:10.1029/2004JA010848.
Scherliess, L., D. C. Thompson, and R. W. Schunk (2008), Longitudinal variability of low-latitude total electron content: Tidal influences, *J. Geophys. Res.*, *113*, A01311, doi:10.1029/2007JA012480.

————————————
F. Ding, L. Liu, B. Ning, W. Wan, J. Xiong, and M.-L. Zhang, Institute of Geology and Geophysics, Chinese Academy of Sciences, Beijing 100029, China. (wanw@mail.iggcas.ac.cn)
X. Pi, Jet Propulsion Laboratory, California Institute of Technology, 4800 Oak Grove Drive, Pasadena, CA 91109, USA.